

Disordering of Fe²⁺ over octahedrally coordinated sites of tourmaline

FERDINANDO BOSI^{1,2,*}

¹Department of Mineralogy, Swedish Museum of Natural History, Box 50007, 10405 Stockholm, Sweden

²Dipartimento di Scienze della Terra, Università di Roma “La Sapienza,” Piazzale Aldo Moro 5, 00185 Roma, Italy

ABSTRACT

The partitioning of iron among octahedrally coordinated sites in tourmaline, and its stereochemical consequences, were investigated in a Fe-rich dravite in a skarn rock from Utö, Sweden. A multi-analytical approach using structure refinement (SREF), electron microprobe analysis (EMPA), and Mössbauer spectroscopy (MS) established the chemical and structural nature of the tourmaline. A structural formula obtained by optimization procedures indicates disordering of Al, Mg, and Fe²⁺ over the Y and Z sites, and ordering of Fe³⁺ at the Y site. Two Fe-rich tourmalines from the literature, re-examined with the optimizing site assignment procedure, appear to have iron partitioning comparable to that of the Utö tourmaline with Fe²⁺ disordered over the octahedral sites. This is best explained by disordered Fe²⁺ distributions that minimize the strain state of the Y-O bonds and provide a shielding effect reducing Y-Z repulsion. This is consistent with predictions from bond-valence theory and Pauling's rules.

An indication of Z-site occupancy by Fe²⁺ in tourmaline may be signaled by a significant correlation between <Z-O> and the *c* lattice parameter ($r^2 = 0.96$). The *c* value for a very Fe²⁺-rich tourmaline and an ideal end-member schorl, with Fe²⁺ and Al ordered at Y and Z (respectively), yielded <Z-O> values larger than 1.907 Å (the likely bond length for <Z-Al-O>). These large <Z-O> lengths indicate that Fe²⁺ occurs at the Z site. The hypothesis of a dragging effect from <Y-O> to explain lengthening of <Z-Al-O> is not supported by experimental evidence.

Keywords: Chemical analysis, tourmaline, crystal structure, Mössbauer spectroscopy, order-disorder, XRD data

INTRODUCTION AND PREVIOUS WORK

The tourmaline group minerals are complex borocyclosilicates that occur in a wide variety of igneous, metamorphic, and sedimentary environments. The structure is characterized by groups of XO₉, YO₆, TO₄, and BO₃ polyhedra connected to each other through ZO₆ octahedra. The latter are arranged in a 3-D framework and are linked to the YO₆ octahedron through the O3-O6 edge. The structural formula of tourmaline group minerals is formalized as XY₃Z₆(T₆O₁₈)(BO₃)₃V₃W and, according to several authors (Fortier and Donnay 1975; MacDonald and Hawthorne 1995; Hawthorne and Henry 1999; Hughes et al. 2004), the following ions fit into the following structural sites: X = Na, Ca, □ (= vacancy), K; Y = Al, Fe³⁺, Cr³⁺, V³⁺, Mg, Fe²⁺, Mn²⁺, Cu²⁺, Zn, Li, Ti⁴⁺, □; Z = Al, Fe³⁺, Cr³⁺, V³⁺, Mg, Fe²⁺; T = Si, Al, B, Be; B = B, (□); W(O1) = OH, F, O; V(O3) = OH, O.

Since 1975, when the first schorl structural refinement was reported by Fortier and Donnay, it has been suggested that Fe²⁺ may occur at the both Y and Z sites of tourmaline. In the following years, Grice and Robinson (1989) reported a structural formula with Fe²⁺ at Y and Z, adding, however, that it was not possible to verify its amount in both the octahedral sites. On the basis of structural data, small amounts of Fe²⁺ at Z (ca. 1% atoms/site) were also reported in Francis et al. (1999) and Ertl and Hughes (2002). Independent indication of the presence of some Fe²⁺ in

the Z site have been obtained in Mössbauer and optical studies, e.g., Burns (1972), Mattson and Rossman (1984), Ferrow et al. (1988), Ferrow (1994), Foit et al. (1989), and Fuchs et al. (1995, 1998). Recently, using an unconstrained model for the assignment of Fe over the octahedral sites of tourmaline, Bosi and Lucchesi (2004) and Bosi et al. (2005b) optimized structural formulae with amounts of Fe²⁺ at Z up to ca. 4% atoms/site. On the bases of the latter structural formulae and the relative peak areas associated with the Mössbauer spectra of the same samples, Andreozzi et al. (2008) found a close match between the amount of Fe²⁺ and Fe³⁺ in Y and Z derived from the structural data and from Mössbauer spectroscopy. Finally, Bosi and Lucchesi (2007) re-examined previously published tourmaline structural formulae using site optimization and found the models are consistent with Fe²⁺ at the Z site.

Nevertheless, the assignment of Fe²⁺ at the Z site still appears controversial. For example, Grice and Ercit (1993) consider only the possibility of Fe³⁺ at the Z site and not Fe²⁺. However, the amounts of ⁵⁷Fe³⁺ reported for their samples 43167, 43293, Cross, 32008, and 43873 corresponds in fact to Fe²⁺. This is verified easily by comparing total Fe²⁺ and Fe³⁺ atoms per formula unit (apfu) from chemical analyses (Table 2 of Grice and Ercit, 1993) with the cation distribution shown in Table 5. Bloodaxe et al. (1999) did not observe the presence of Fe²⁺ at the Z site, and their results are often extrapolated to other Fe-tourmalines (e.g., Oliveira et al. 2002; Pieczka and Kraczka 2004). However, it should be noted that the samples of Bloodaxe et al. (1999) pos-

* E-mail: ferdinando.bosi@uniroma1.it

sess an electron occupancy at the *Z* site between 12 and 13 e^- , in agreement with Al and Mg occupancy. Assuming their cation distribution scheme to be “definitive” is hazardous, since not all Fe-tourmalines have less than 13 e^- in *Z*. In fact, other alternatives could be considered rather than make the assumption of Fe^{2+} exclusively at the *Y* site. Therefore, it is important to stress the point about the site occupancy of Fe^{2+} . After Hawthorne et al. (1993) had shown the presence of Mg at the *Z* site of tourmaline, it was clear that the ZO_6 octahedron could enlarge to host non-Al cations. This result was important, because it highlights the fact that the usual assumption—that Al completely fills the *Z* site before occupying any other site—is not correct. Consequently, it should be not surprising if other divalent cations, such as Fe^{2+} , may occur at the *Z* site, in proportions related to *Z*-site cation size mismatch.

This study presents chemical and structural data of a single crystal of Fe-bearing tourmaline. These data in conjunction with literature data are used to clarify the crystal-chemical mechanisms for which Fe^{2+} may be disordered over the octahedrally coordinated sites of tourmaline.

OCCURRENCE

The tourmaline crystal under investigation is from the Swedish Museum of Natural History (collection number 19980432). It occurs in a skarn rock from the island of Utö (south of Stockholm, Sweden). The bedrock of Utö is mainly characterized by Proterozoic metatuffitic rocks, gabbro-granitic intrusions, layered quartz porphyry intrusions, a banded iron formation, and metasedimentary rocks with associated marbles, and skarns (Stålhös 1982). Several granitic pegmatite dikes transect the Utö rocks, and tourmaline frequently occurs in the classic petalite-subtype pegmatites (e.g., Selway et al. 2002). An unusual black tourmaline, associated with tennantite as the dominant phase, with minor chalcopyrite and bornite, was found in a small cavity filled with calcite in an iron mine on Utö. Therefore, this sample is not the typical Utö tourmaline, but rather represents a late skarn-forming phase (Dan Holtstam, pers. comm.).

ANALYTICAL AND CRYSTAL STRUCTURAL PROCEDURES

Single-crystal structural refinement (SREF)

After preliminary optical examination, one representative crystal fragment was selected for X-ray data collection with a four-circle Siemens P4 automated diffractometer. Unit-cell parameters were measured by centering 52 reflections (13 independent reflections and their Friedel pairs, on both sides of the direct beam) in the range $85-95^\circ 2\theta$, with $MoK\alpha$ radiation (0.70930 Å). X-ray data were collected in the $3-70^\circ 2\theta$ range with the ω -scan method. Scan speed was variable, depending on reflection intensity, estimated with a pre-scan. Background was measured with a stationary crystal and counter at the beginning and end of each scan, in both cases for half the scan time. Preliminary full exploration of reciprocal space was carried out, and no violations of $R3m$ symmetry were noted. Data reduction was performed with the SHELXTL-PC program package. Intensities were corrected for polarization and Lorentz effects. An absorption correction was accomplished with a semi-empirical method (North et al. 1968). Structure refinement was carried out with the SHELXL-97 program (Sheldrick 1997). Starting coordinates were taken from Foit (1989). Variable parameters were scale factor, extinction coefficient, Flack parameter, atomic coordinates, site scattering values expressed as mean atomic number of *X*, *Y*, and *Z* sites, and atomic displacement factors. The *X* site was modeled using Na scattering factors. The occupancies of the *Y* site were obtained considering the presence of Mg vs. Fe, and the occupancy of *Z* site considering Al. The *T* and *B* sites were modeled with Si and B scattering factors, respectively, and with fixed occupancy of 1, because refinement with unconstrained multiplicity showed the *T* and *B* sites to be fully occupied by Si and B, respectively. The H atom associated with O3 (H3) was found by difference Fourier synthesis, and

subsequently refined. Three isotropic, full-matrix, refinement cycles were followed by anisotropic cycles until convergence was attained. No correlation between scale factor and site occupancy was observed. Table 1 lists crystal data, data-collection information and refinement details, and Table 2 gives the fractional atomic coordinates and equivalent isotropic displacement parameters. Table 3¹ contains anisotropic displacement parameters for non-hydrogen atoms. Relevant bond lengths, octahedral and tetrahedral distortions (expressed as mean quadratic elongation; Robinson et al. 1971), and mean atomic number are listed in Table 4.

Electron microprobe analysis (EMPA)

After X-ray data collection, the same crystal was mounted on a glass slide, polished and carbon-coated for electron microprobe analysis (WDS-EDS method) on a CAMECA SX50 electron microprobe, operating at 15 kV, sample current of 15 nA, and with a beam diameter of 5 μ m. For raw data reduction, the PAP computer

TABLE 1. Miscellaneous X-ray data of the refinement of the Utö tourmaline

Crystal data	
Space group	<i>R3m</i>
<i>Z</i>	3
<i>a</i> (Å)	15.9875(8)
<i>c</i> (Å)	7.2372(5)
<i>V</i> (Å ³)	1602.0(2)
Crystal size (mm)	0.12 × 0.11 × 0.13
Diffraction intensity collection	
Radiation	$MoK\alpha$ (0.71073 Å)
Monochromator	High-crystallinity graphite crystal
Range	$3-70^\circ 2\theta$
Reciprocal space range	$0 \leq h, k \leq 26, -12 \leq l \leq 12$
Scan method	ω
Scan range	2.4°
Scan speed	Variable 1.5–14.6 $^\circ$ /min
Temperature	296 K
Data reduction	
Program	SHELXTL-PC
Corrections	Lorentz, Polarization
Absorption correction	Semi-empirical, 13 Ψ scans ($10-70^\circ 2\theta$)
Set of measured reflections	1711
Refinement	
Program	SHELXL-97
<i>wR2</i> (%)	5.01
<i>R1</i> (%) for $I_o > 2\sigma(I_o)$	2.26
Goof	1.056
Extinction coefficient	0.0039(2)
Flack parameter	0.02(2)
Largest diff. peak and hole ($e/\text{Å}^3$)	0.40 and -0.37

TABLE 2. Fractional coordinates and equivalent displacement factor (Å^2)

Site	<i>x</i>	<i>y</i>	<i>z</i>	U_{eq}
<i>X</i>	0	0	0.22803(21)	0.0121(4)
<i>Y</i>	0.12314(4)	<i>x</i> /2	0.63654(8)	0.0072(1)
<i>Z</i>	0.29818(3)	0.26182(3)	0.61179(8)	0.0054(1)
<i>B</i>	0.11004(8)	2 <i>x</i>	0.45391(32)	0.0067(3)
<i>T</i>	0.19155(3)	0.18979(3)	0	0.00500(8)
O1 (<i>W</i>)	0	0	0.77405(41)	0.0118(5)
O2	0.06076(6)	2 <i>x</i>	0.48109(24)	0.0099(3)
O3 (<i>V</i>)	0.26447(13)	<i>x</i> /2	0.51197(24)	0.0115(3)
O4	0.09254(6)	2 <i>x</i>	0.07090(23)	0.0098(3)
O5	0.18277(12)	<i>x</i> /2	0.09062(23)	0.0099(3)
O6	0.19543(8)	0.18604(8)	0.77857(16)	0.0084(2)
O7	0.28443(8)	0.28420(8)	0.07916(16)	0.0087(2)
O8	0.20917(8)	0.26991(8)	0.44095(18)	0.0102(2)
H3	0.2510(30)	<i>x</i> /2	0.3888(57)	0.04(1)

¹ Deposit item AM-08-051, Table 3 and CIF. Deposit items are available two ways: For a paper copy contact the Business Office of the Mineralogical Society of America (see inside front cover of recent issue) for price information. For an electronic copy visit the MSA web site at <http://www.minsocam.org>, go to the American Mineralogist Contents, find the table of contents for the specific volume/issue wanted, and then click on the deposit link there.

TABLE 4. Relevant bond lengths (Å), mean quadratic elongation ($\langle\lambda\rangle$) for the octahedra and tetrahedron, and mean atomic number (m.a.n.)

B-O2	1.379(3)	Y-O1	1.974(2)
B-O8 (×2)	1.376(2)	Y-O2 (×2)	2.033(1)
<B-O>	1.377(2)	Y-O3	2.154(2)
m.a.n. B	5	Y-O6 (×2)	2.013(1)
		<Y-O>	2.037(1)
T-O4	1.6296(6)	<λ> _Y	1.0218
T-O5	1.6445(8)	m.a.n. Y	17.81(8)
T-O7	1.603(1)		
T-O6	1.606(1)	Z-O3	1.9969(9)
<T-O>	1.621(1)	Z-O6	1.906(1)
<λ> _T	1.0030	Z-O8	1.938(1)
m.a.n. T	14	Z-O7E*	1.915(1)
		Z-O7D*	1.971(1)
X-O2 (×3)	2.487(2)	Z-O8E*	1.904(1)
X-O4 (×3)	2.803(2)	<Z-O>	1.938(1)
X-O5 (×3)	2.719(2)	<λ> _Z	1.0134
<X-O>	2.670(2)	m.a.n. Z	13.56(4)
m.a.n. X	13.1(1)		
		O3-H	0.91(4)

* According to labels reported in Foit (1989).

TABLE 5. Chemical composition of the present Utö tourmaline

	wt%		apfu
SiO ₂	36.7(2)	Si	6.00(5)
TiO ₂	0.07(2)	Ti ⁴⁺	0.009(3)
B ₂ O ₃ *	10.63	B	3.00
Al ₂ O ₃	27.48(5)	Al	5.30(4)
FeO	10.5(4)	Fe ³⁺	0.85(3)
MnO	0.17(3)	Fe ²⁺	0.59(2)
MgO	9.18(5)	Mn ²⁺	0.023(4)
CaO	1.63(4)	Mg	2.24(2)
Na ₂ O	2.01(5)	Ca	0.286(8)
K ₂ O	0.07(1)	Na	0.64(2)
F	0.15(4)	K	0.014(2)
H ₂ O*	3.24	F	0.08(2)
O = F	-0.065	OH	3.54
Total	101.7	OH + F	3.62
Fe ₂ O ₃ †	6.88	Sum Y + Z‡	9.00
FeO†	4.30	X-vacancy	0.06

Notes: Number of ions calculated on basis of 31 (O, OH, F). Uncertainties for oxides (in parentheses) are standard deviation of repeated analyses. B₂O₃ and H₂O uncertainty assumed at 5%. Standard uncertainty for ions was calculated by uncertainty-propagation theory.

* Calculated by stoichiometry.

† From MS data (Table 6).

‡ Using three decimals.

program was applied (Pouchou and Pichoir 1984). Natural and synthetic standards were used: anorthite (Al), rutile (Ti), olivine (Si, Fe), rhodonite (Mn), diopside (Mg, Ca), sphalerite (Zn), orthoclase (Na, K), fluorite (F), synthetic metals (Cr, V, Cu). Each element determination was accepted after checking that the intensity of the analyzed standard before and after each determination was within 1%. The chemical composition data are the average of 10 spot analyses, performed along two orthogonal traverses, and their standard deviations indicate compositional homogeneity (Table 5). In accordance with the documented very low concentration of Li in dravitic samples (Dyar et al. 1998) and the absence of Li-enriched minerals, the Li₂O content was assumed to be insignificant. ZnO, CuO, V₂O₃, and Cr₂O₃ were not detected, with their concentrations being below the minimum detection limits of 0.03 wt%.

Mössbauer spectroscopy (MS)

A Mössbauer spectrum was collected at 25 °C using a conventional spectrometer system operating in constant acceleration mode with a ⁵⁷Co point-source of 10 mCi in a rhodium matrix. The absorber consisted of 1.6 mg powdered tourmaline placed between mylar windows in an aperture (1 mm diameter) in a lead metal disk. The Fe thickness of the absorber was ca. 7 mg/cm². Data collection time was about one week for robust statistics. Spectral data for the velocity range -4 to +4 mm/s were recorded on a multichannel analyzer using 1024 channels. After velocity calibration against a spectrum of high-purity α-iron foil (0.25 mm thick),

the raw data were reduced to 512 and then folded to 256 channels. The folded spectrum showed very weak peaks at about -3.1 and +3.6 mm/s indicating the presence of small amounts of a magnetic phase in the spectrum. Consequently, a second spectrum was recorded in the range -10 to +10 mm/s to assess the amount and identity of this impurity. Inspection of this Mössbauer spectrum indicated the presence of strong non-magnetic absorption (tourmaline) and very weak magnetic absorption, which according to Mössbauer parameters is chalcopyrite (Table 6). Because the chalcopyrite absorption is a sextet, its contribution to the central part of the spectrum (from -2 to 3 mm/s) is below 1%. Hence, the chalcopyrite contamination of the tourmaline spectrum is considered negligible.

The original spectrum was fitted assuming Lorentzian peak shape, using a

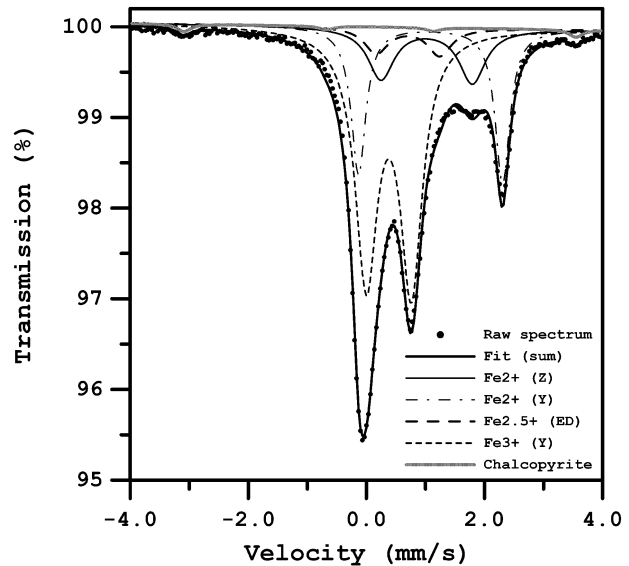


FIGURE 1. Room-temperature Mössbauer spectrum of the Utö tourmaline. Spectral data were recorded in the velocity range -10 to 10 mm/s to evaluate the chalcopyrite contribution to the tourmaline spectrum. Because this contribution is very weak, in figure displays only the spectrum recorded in the velocity range -4 to 4 mm/s. ED = electron delocalization.

TABLE 6. Mössbauer parameters of the Utö tourmaline

Fe valence	Parameter	Value	Amount of Fe in tourmaline sites (pfu)	Assignment
Fe ²⁺	δ	1.02	0.21	Z site
	ΔE _Q	1.55		
	Γ	0.53		
	% Area	14 ± 3		
Fe ²⁺	δ	1.09	0.32	Y site
	ΔE _Q	2.44		
	Γ	0.29		
	% Area	22 ± 1		
Fe ^{2.5+}	δ	0.70	0.08	Z site
	ΔE _Q	1.08		
	Γ	0.49		
	% Area	6 ± 2		
Fe ³⁺	δ	0.38	0.79	Y site
	ΔE _Q	0.76		
	Γ	0.44		
	% Area	56 ± 1		
Chalcopyrite	δ	0.23		
	ΔE _Q	0		
	Γ	0.28		
	H*	35.6		
	% Area	2 ± 1		

Notes: δ, ΔE_Q, and Γ are in mm/s. Errors on these parameters are ±0.02 mm/s.

* H = Hyperfine magnetic field (Tesla), error is ±1 (T).

least squares fitting program (Jernberg and Sundqvist 1983). Reduced χ^2 was considered as a parameter to evaluate statistical best fit. Four doublets and a sextet were used as a fitting strategy (Fig. 1), and the χ^2 was 1.41. The addition of another doublet yielded slight reduction in χ^2 , but some refined hyperfine parameters were unrealistic and, therefore, the above strategy was preferred. Errors were estimated at ± 0.02 mm/s for isomer shift (δ), quadrupole splitting (ΔE_Q) and peak width (Γ), and ± 1 –3% for absorption areas due to doublet overlap (Table 6). Figure 1 shows that Fe^{3+} is the principal oxidation state, followed by Fe^{2+} and $\text{Fe}^{2.5+}$ (electron delocalization), and that all iron is in octahedral coordination. Contents of FeO and Fe_2O_3 (Table 5) were obtained from $\text{Fe}^{2+}/\text{Fe}^{3+}$ ratios measured by MS.

RESULTS AND DISCUSSION

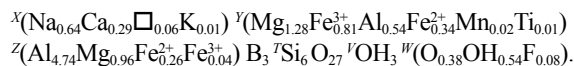
Determination of atomic proportions

Structure refinement shows that the *B* and *T* sites are filled by B and Si, respectively. The latter information is consistent with EMPA data. Consequently, atomic proportions were calculated assuming stoichiometric B. All Mn was assumed to be divalent, as not all iron was oxidized, and crystal-structure studies have shown that this is the most common valence state of Mn in tourmaline (Bosi et al. 2005a). In this way, the OH content can be calculated by charge balance with the assumption $Y + Z = 9.00$ apfu. It is possible to verify the amount of OH by considering the F content and the bond valence sum at O1 (Grice and Ercit 1993). Because bond lengths reflect bond valence values, the latter can be evaluated by a first approximation of the atomic distribution. For the Utö tourmaline, the bond-valence sum at O1 is 1.44 valence units (calculated according to Brown and Altermatt 1985), which yields an OH amount of 3.5 apfu in excellent agreement with the inferred by stoichiometry (Table 5).

According to the classification of Hawthorne and Henry (1999), this skarn tourmaline belongs to the alkali group: the *X* site is dominated by Na, with 0.64 apfu. The amount of Mg (2.24 apfu) is larger than Fe (1.44 apfu), with Fe^{3+} (0.85 apfu) larger than Fe^{2+} (0.59 apfu). Consequently, the Utö sample may be classified as a Fe-rich dravite.

Determination of site population

To convert crystal chemical and structure-refinement results into accurate site populations, optimization between experimental and calculated data from atomic distribution should be achieved. Bosi and Lucchesi (2007) used a quadratic program approach to minimize the residuals between calculated and observed data from chemical analysis and structure refinement to re-examine the cation distributions of several tourmaline specimens. They showed that a self-consistent set of ionic radii fits the *T*-, *Y*-, and *Z*-mean bond lengths of most of the refined tourmaline specimens in the literature. This approach was employed for obtaining the cation distribution of the *Y* and *Z* sites in the Utö sample. All residuals between calculated and observed data (such as mean atomic number, mean bond lengths, atomic proportions) are within analytical error (two standard deviations). The final structural formula of the Utö tourmaline is



This formula shows a clear disordering of Al, Mg, and Fe^{2+} over the *Y* and *Z* sites, and strong ordering of Fe^{3+} at the *Y* site. Although Fe^{2+} seems to prefer the *Y* site, a significant amount

of Fe^{2+} is found in *Z*. This iron partitioning is also in accordance with that reported by Fortier and Donnay (1975) and by Bosi and Lucchesi (2004).

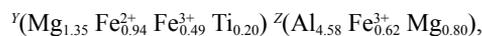
Mössbauer data

Mössbauer spectra of tourmaline are often complex and their interpretation is not straightforward. As a rule, Mössbauer data used to characterize relative site-occupancies for Fe, when combined with chemical analysis results, should provide absolute occupancies in agreement with those derived from structure refinement. In the Utö tourmaline, the assignment of the Fe doublets to the *Y* or *Z* sites is not possible solely on the basis of Mössbauer parameters because several models may be assumed. However, taking into account the areas of the Fe^{2+} , $\text{Fe}^{2.5+}$, and Fe^{3+} doublets, only one model is consistent with the structural data: that is the model reported in Table 6. The case of Fe^{3+} nicely illustrates this. Assignment of the absorption areas of the Fe^{3+} doublet (56% of Fe_{tot}) to the *Z* site will yield a residual between calculated and observed site scatterings at the *Y* and *Z* sites much larger ($>1.10 e^-$) than their analytical error (Table 4). In contrast, the assignment of this Fe^{3+} doublet to the *Y* site fits significantly better with the site-occupancy refinement (residuals $<0.12 e^-$). Hence, the Fe^{3+} doublet is consistent with assignment to the *Y* site. The two doublets assigned to Fe^{2+} , distinguished by their ΔE_Q values, represent Fe^{2+} in different structural environments: because the YO_6 distortion ($\langle\lambda_Y\rangle = 1.0218$) is larger than the ZO_6 distortion ($\langle\lambda_Z\rangle = 1.0134$), the former is reflected in the larger $\Delta E_Q = 2.44$ mm/s (assigned to *Y*, in accordance with the optimized structural formula) and the latter in the smaller $\Delta E_Q = 1.55$ mm/s (assigned to *Z*, in accordance with the optimized structural formula). The positive correlation between ΔE_Q for Fe^{2+} and octahedral distortion is consistent with published results for Fe^{2+} in weakly distorted ($\langle\lambda\rangle \leq 1.02$) octahedra (Zhe and De Grave 1998). The $\text{Fe}^{2.5+}$ doublet is related to interaction between Fe^{3+} and Fe^{2+} located in *Z*-*Z* (although a minor interaction *Y*-*Z* might occur, which is within analytical error); this assignment is also supported by the results of Farrow (1994) and Andreozzi et al. (2008).

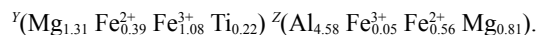
Reconsideration of previously published crystal-chemical formulae

Because the Utö sample is most consistent with Fe^{3+} at *Y* and Fe^{2+} at *Z*, it is worth considering whether other Fe-bearing tourmaline specimens from the literature, for which Fe^{2+} at the *Z* site is not reported, also have similar iron partitioning. Samples drv18 of Cámara et al. (2002) and GRAS1 of Ertl et al. (2006) illustrate this possibility. The cation distributions of drv18 and GRAS1 were re-examined using the same procedure adopted for the Utö sample.

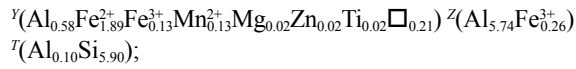
For sample drv18, the original cation distribution (Cámara et al. 2002) was reported as



and the newly optimized one is



For sample GRAS1, the original cation distribution (Ertl et al. 2006) was reported as



and the new one is

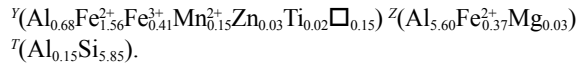


Figure 2 displays the optimization residuals between observed and calculated data from the original and new cation distributions in the two cases. There is a clear improvement in the new site assignment, with a better distribution of minimal residuals over the whole structure. For example, the site scattering residuals retrieved from the original cation distributions for the *Y* and *Z* sites (ca. -0.33 and 0.23 e^- in drv18 and GRAS1, respectively) are much greater than their uncertainties (0.10 and 0.04 e^- , respectively). In contrast, the optimized parameters in the new cation distributions are within analytical error. Notably, the main difference between the original and new cation distribution of the drv18 and GRAS1 is the presence of significant amounts of Fe^{2+} at the *Z* sites (ca. 9 and 6% atoms/site, respectively).

STERIC REASONS FOR IRON PARTITION BETWEEN BOTH OCTAHEDRAL SITES

Bond valence approach

The preference of Fe^{2+} over Fe^{3+} at the *Z* site and, conversely Fe^{3+} over Fe^{2+} at the *Y* site, may be explained by considering

the difference between mean atomic valence (MAV) and bond valence sum (BVS) at the *Y* site: i.e., *Y*-site valence residuals in Figure 2. Using the original cation distributions of drv18 and GRAS1, this difference is larger than -0.18 valence unit (v.u.). This suggests an underbonded state in the *Y* site because the MAV obtained from the original cation distribution does not match the BVS obtained by the experimental *Y*-O bond lengths. According to the bond valence theory, there is a tendency for experimental bond valences around each atom to approach atomic valence (equal-valence rule). Large mismatches between MAV and BVS are indicative of strained bonds, which may lead to instabilities in the structure. Consequently, any structure tends to relax its bonds to minimize the strain (Brown 2002). Incorporating Fe^{3+} (instead of Fe^{2+}) into the *Y* site, *Y*-O bond lengths decrease and *Y* MAV increases. As a result, the deviation from the equal-valence rule decreases and the *Y*-O bonds tend to relax. This is consistent with the new cation distributions (Fig. 2).

Structural constraints

The preference of Fe^{2+} over Fe^{3+} at *Z* and, conversely, Fe^{3+} over Fe^{2+} at *Y* appears to be a function of size and charge required at the *Y* site. Relationships between structural parameters and compositional parameters illustrate how the tourmaline structure exerts constraints on its own chemical composition, i.e., maintaining the difference between $\langle Y-O \rangle$ and $\langle Z-O \rangle$ (Δ_{YZ}) smaller than ca. 0.15 Å (Bosi and Lucchesi 2007). A substitution like ${}^Y\text{Al} + {}^Z\text{R}^{2+} \rightarrow {}^Y\text{R}^{2+} + {}^Z\text{Al}$ increases the structural stability because it decreases Δ_{YZ} ($\langle Y-O \rangle$ decreases and $\langle Z-O \rangle$ increases).

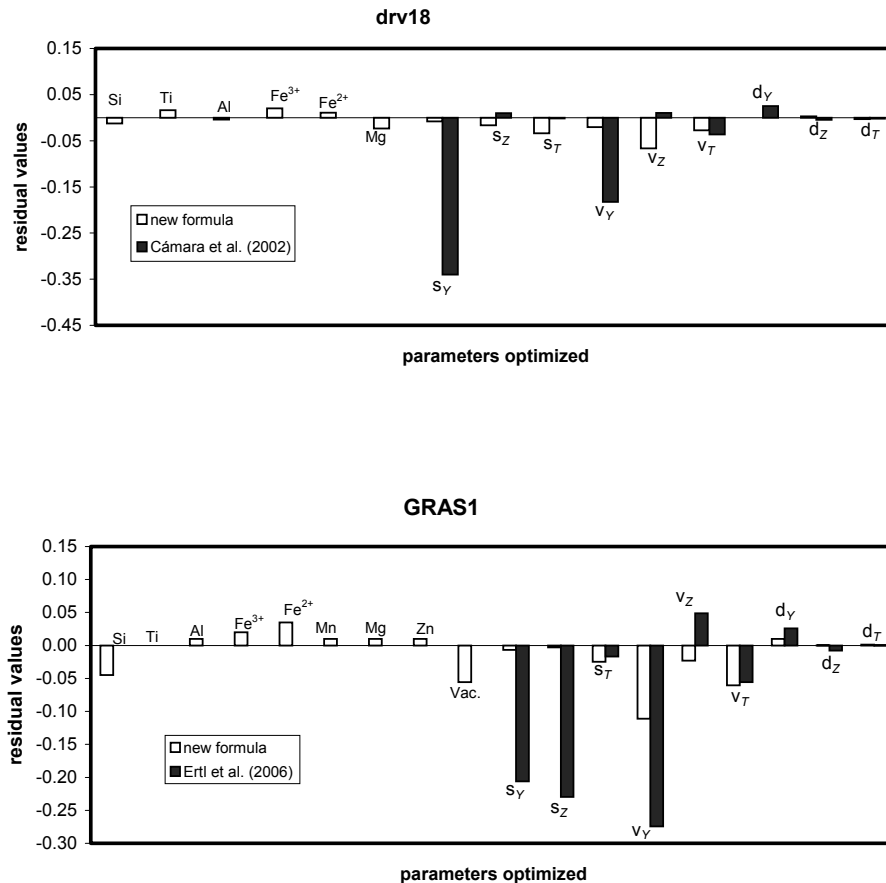


FIGURE 2. Plot of residuals (calculated – observed) for optimized parameters: s_Y , s_Z , and s_T = site scattering; v_Y , v_Z , v_T = site valence; d_Y , d_Z , d_T = mean bond length.

This mechanism is further supported by the observed positive correlation between the O3-Z-O6 angle, which is opposite to the O3-O6 edge shared between *Y* and *Z*, and Δ_{YZ} (Fig. 3). For the tourmaline structure, this correlation represents a strong constraint whereby $\langle Y-O \rangle$ maintains dimensions commensurate with $\langle Z-O \rangle$. If the O3-Z-O6 angle becomes larger, the shielding effect of the anions is weakened and the repulsive force between *Y* and *Z* becomes greater. This may lead to instabilities in the structure (Pauling's rules). Incorporating Fe^{3+} into *Y* and Fe^{2+} into *Z* (for example by ${}^YFe^{3+} + {}^ZFe^{2+} \rightarrow {}^YFe^{2+} + {}^ZFe^{3+}$), both Δ_{YZ} and O3-Z-O6 decrease. In this way, the shielding effect needed to reduce the *Y-Z* repulsion is provided, and the structural state moves toward a free energy minimum.

According to the ionic radii reported by Bosi and Lucchesi (2007), the Δ_{YZ} values calculated for the ideal schorl ($\dots {}^YFe_3^2+ {}^ZAl_6 \dots$) and dravite ($\dots {}^YMg_3 {}^ZAl_6 \dots$), yield large O3-Z-O6 values. The model of Bosi and Lucchesi (2007) indicates that these ordered schorl and dravite end-members should be unstable (Fig. 3). Stability of schorl and dravite may increase by disordering of Mg, Fe and Al over the octahedral sites, which yields decreasing Δ_{YZ} as well as O3-Z-O6. As a consequence, the absence of ordered schorl and dravite end-members in nature may be ascribed to crystal-chemical constraints rather than to petrologic conditions.

Variations in mean bond length due to constituent anions are very small compared to those due to constituent cations in tourmaline, therefore anions could take part in the above-mentioned disordering scheme.

Use of the *c* lattice parameter to evaluate $\langle Z-O \rangle$

A plot of $\langle Z-O \rangle$ vs. *c* for 129 crystal-structural refinements of tourmaline samples spanning the whole tourmaline group shows a positive correlation (Fig. 4). The following quadratic fit is obtained:

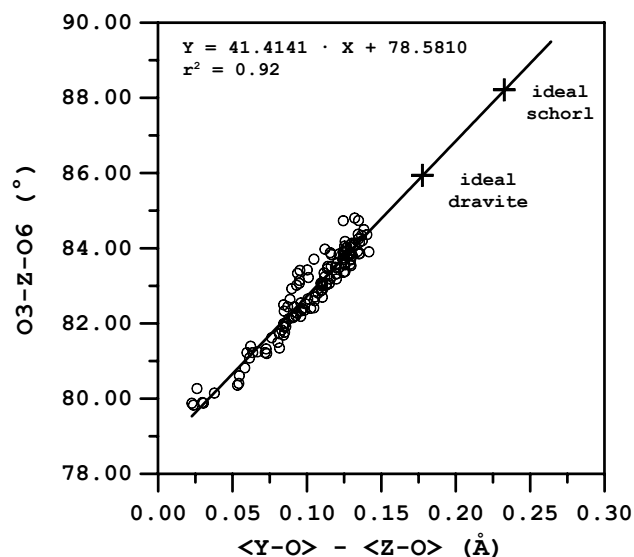


FIGURE 3. Variation in the O3-Z-O6 angle as a function of the difference between $\langle Y-O \rangle$ and $\langle Z-O \rangle$ in tourmaline. Plot obtained using 129 samples: 127 from literature (see references in Bosi and Lucchesi 2007) plus the Utö and GRAS1 samples.

$$\langle Z-O \rangle = 0.47467 \times c^2 - 6.5626 \times c + 24.5720.$$

This relation can be used to predict $\langle Z-O \rangle$ values from lattice parameter measurements and obtain information on *Z*-site occupancy. For example, the schorl reported in JCPDF (number 43-1464) shows very high amounts of Fe^{2+} (2.48 apfu) and the *c*-lattice parameter is 7.172 Å. The ideal end-member schorl ($\dots {}^YFe_3^2+ {}^ZAl_6 \dots$) reported by Pieczka (2000), has a *c*-lattice parameter of 7.206 Å. Replacing these two *c* values in the above quadratic fit, $\langle Z-O \rangle$ values of 1.921 and 1.930 Å, respectively, are obtained. However, in the ideal end-member schorl, with Fe^{2+} and Al ordered at the *Y* and *Z* sites, respectively, the most reasonable bond length for $\langle {}^ZAl-O \rangle$ is 1.907 Å. In fact, this bond length is consistent with: (1) $\langle Z-O \rangle$ average calculated from 35 tourmalines from the literature, in which the *Z* site is only occupied by Al (Fig. 5); (2) $\langle {}^ZAl-O \rangle$ bond length refined by Bosi et al. (2005a, 2005b) in tourmaline with $\Sigma {}^ZR^{2+} < 0.40$ apfu; and (3) $\langle {}^ZAl-O \rangle$ calculated on the basis of the bond valence constant and coordination number related to ${}^VIAl^{3+}$: i.e., $1.651 - 0.37 \times \ln(3/6) = 1.907$ Å. To explain the larger $\langle Z-O \rangle$ values (1.921 and 1.930 Å) obtained by using the data of JCPDS and Pieczka (2000), we may assume a dragging effect of $\langle Y-O \rangle$ that lengthens $\langle {}^ZAl-O \rangle$; alternatively, significant amounts of Fe^{2+} may be present at the *Z* site. In the former hypothesis, a direct proportionality relation between $\langle Y-O \rangle$ and $\langle {}^ZAl-O \rangle$ should exist. However, the plot of $\langle Y-O \rangle$ vs. $\langle Z-O \rangle$ in 35 tourmalines with ${}^ZAl = 6$ apfu shows no such correlation (Fig. 5). Furthermore, any polyhedron with fixed composition should exhibit an increase in size with increasing distortion (e.g., Brown 2002). Consequently, if $\langle Y-O \rangle$ and $\langle Z-O \rangle$ are linked by a direct proportionality relation, $\langle Y-O \rangle$ should be positively correlated with ZO_6 distortion. In contrast, a strong negative correlation ($r^2 = 0.92$) exists between $\langle Y-O \rangle$ and ZO_6 distortion (Bosi and Lucchesi 2007). This inverse proportionality relation indicates that, when $\langle Y-O \rangle$ increases, the ZO_6 polyhedron becomes more regular. As a result, $\langle Z-O \rangle$ tends to decrease, as expected from the tendency of *Y* to compress *Z* (Foit 1989; Bosi and Lucchesi 2007). In the tourmaline group, it makes no crystal-chemical sense to explain a $\langle Z-O \rangle$ variation by

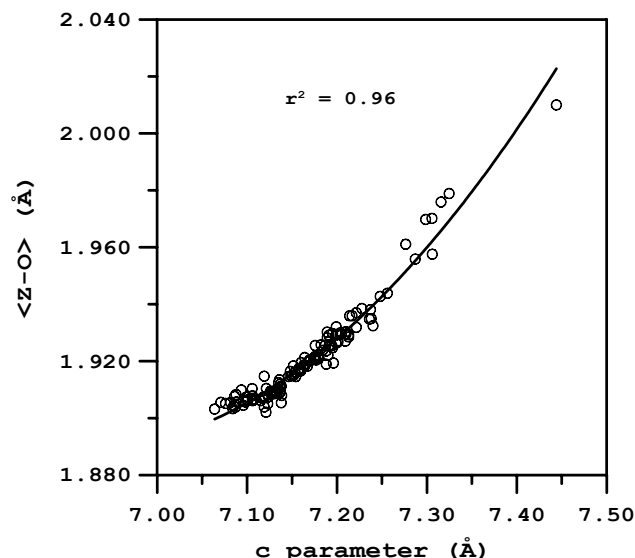


FIGURE 4. $\langle Z-O \rangle$ vs. *c*-cell edge, showing strong dependence of these structural parameters. Plot obtained using the same as in Figure 3.

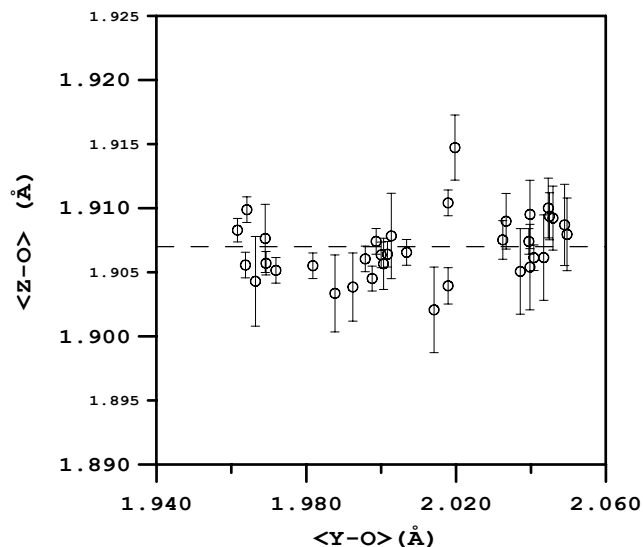


FIGURE 5. Plot of 35 tourmalines with Al = 6 apfu from literature (see references in Bosi and Lucchesi 2007), showing that no correlation of direct proportionality exists between Z and Y mean bond lengths ($r^2 < 0.06$). Dotted horizontal line: average of $\langle Z-O \rangle = 1.907(2)$ Å. Vertical bars: average estimated standard deviation ($\pm 1\sigma$).

direct proportionality with $\langle Y-O \rangle$, when it may be explained by a compositional variation of the Z population. Larger $\langle Z-O \rangle$ values obtained for the very Fe²⁺-rich schorl reported in JCPDS and the ideal end-member schorl of Pieczka (2000) strongly suggest the presence of Fe²⁺ (associated with Al) at the Z site.

In conclusion, a careful examination of some Fe-tourmalines demonstrates that limited, but significant, amounts of Fe²⁺ are required at the Z site. This is consistent with analytical data, the bond-valence theory, and Pauling's rules.

ACKNOWLEDGMENTS

I am indebted to U. Hälenius for the Mössbauer spectrum collection, helping in interpretation and useful suggestions, to S. Lucchesi, G.B. Andreozzi, and D. Henry for the valuable comments to the text. I also thank an anonymous reviewer and G.R. Rossman for reviews.

REFERENCES CITED

Andreozzi, G.B., Bosi, F., and Longo, M. (2008) Linking Mössbauer and structural parameters in elbaite-schorl-dravite tourmalines. *American Mineralogist*, 93, 658–666.

Bloodaxe, E.S., Hughes, J.M., Dyar, M.D., Grew, E.S., and Guidotti, C.V. (1999) Linking structure and chemistry in the schorl-dravite series. *American Mineralogist*, 84, 922–928.

Bosi, F. and Lucchesi, S. (2004) Crystal chemistry of the schorl-dravite series. *European Journal of Mineralogy*, 16, 335–344.

——— (2007) Crystal chemical relationships in the tourmaline group: Structural constraints on chemical variability. *American Mineralogist*, 92, 1050–1063.

Bosi, F., Agrosi, G., Lucchesi, S., Melchiorre, G., and Scandale, E. (2005a) Mn-tourmaline from island of Elba (Italy): Crystal chemistry. *American Mineralogist*, 90, 1661–1668.

Bosi, F., Andreozzi, G.B., Federico, M., Graziani, G., and Lucchesi, S. (2005b) Crystal chemistry of the elbaite-schorl series. *American Mineralogist*, 90, 1784–1792.

Brown, I.D. (2002) The chemical bond in inorganic chemistry: the bond valence model, 288 p. International Union of Crystallography Monographs on Crystallography, 12, Oxford University Press, New York.

Brown, I.D. and Altermatt, D. (1985) Bond-valence parameters obtained from a systematic analysis of the Inorganic Crystal Structure Database. *Acta Crystallographica*, B41, 244–247.

Burns, R.G. (1972) Mixed valencies and site occupancies of iron in silicate minerals from Mössbauer spectroscopy. *Canadian Journal of Spectroscopy*, 17, 51–59.

Cámara, F., Ottolini, L., and Hawthorne, F.C. (2002) Crystal chemistry of three tourmalines by SREF, EMPA, and SIMS. *American Mineralogist*, 87,

1437–1442.

Dyar, M.D., Taylor, M.E., Lutz, T.M., Francis, C.A., Guidotti, C.V., and Wise, M. (1998) Inclusive chemical characterization of tourmaline: Mössbauer study of Fe valence and site occupancy. *American Mineralogist*, 83, 848–864.

Ertl, A. and Hughes, J.M. (2002) The crystal structure of an aluminum-rich schorl overgrown by boron-rich olenite from Koralpe, Styria, Austria. *Mineralogy and Petrology*, 75, 69–78.

Ertl, A., Kolitsch, U., Prowatke, S., Dyar, M.D., and Henry, D.J. (2006) The Fe-analog of schorl from Grasstein, Trentino–South Tyrol, Italy: crystal structure and chemistry. *European Journal of Mineralogy*, 18, 583–588.

Ferrow, E.A. (1994) Mössbauer effect study of the crystal chemistry of tourmaline. *Hyperfine Interactions*, 91, 689–695.

Ferrow, E.A., Annersten, H., and Gunawardane, R.P. (1988) Mössbauer effect study on the mixed valence state of iron in tourmaline. *Mineralogical Magazine*, 52, 221–228.

Foit Jr., F.F. (1989) Crystal chemistry of alkali-deficient schorl and tourmaline structural relationships. *American Mineralogist*, 74, 422–431.

Foit Jr., F.F., Fuchs, Y., and Myers, P.E. (1989) Chemistry of alkali-deficient schorls from two tourmaline-dumortierite deposits. *American Mineralogist*, 74, 1317–1324.

Fortier, S. and Donnay, G. (1975) Schorl refinement showing composition dependence of the tourmaline structure. *Canadian Mineralogist*, 13, 173–177.

Francis, C.A., Dyar, M.D., Williams, M.L., and Hughes, J.M. (1999) The occurrence and crystal structure of foitite from a tungsten-bearing vein at Copper Mountain, Taos County, New Mexico. *Canadian Mineralogist*, 37, 1431–1438.

Fuchs, Y., Lagache, M., Linares, J., Maury, R., and Varret, F. (1995) Mössbauer and optical spectrometry of selected schorl-dravite tourmalines. *Hyperfine Interactions*, 96, 245–258.

Fuchs, Y., Lagache, M., and Linares, J. (1998) Fe-tourmaline synthesis under different *T* and *f*_{o₂} conditions. *American Mineralogist*, 83, 525–534.

Grice, J.D. and Ercit, T.S. (1993) Ordering of Fe and Mg in the tourmaline crystal structure: The correct formula. *Neues Jahrbuch für Mineralogie Abhandlungen*, 165, 245–266.

Grice, J.D. and Robinson, G.W. (1989) Feruvite, a new member of the tourmaline group, and its crystal structure. *Canadian Mineralogist*, 27, 199–203.

Hawthorne, F.C. and Henry, D. (1999) Classification of the minerals of the tourmaline group. *European Journal of Mineralogy*, 11, 201–215.

Hawthorne, F.C., MacDonald, D.J., and Burns, P.C. (1993) Reassignment of cation occupancies in tourmaline: Al-Mg disorder in the crystal structure of dravite. *American Mineralogist*, 78, 265–270.

Hughes, J.M., Ertl, A., Dyar, M.D., Grew, E.S., Wiedenbeck, M., and Brandstätter, F. (2004) Structural and chemical response to varying ⁷B content in zoned Fe-bearing olenite from Koralpe, Austria. *American Mineralogist*, 49, 447–454.

Jernberg, P. and Sundqvist, T. (1983) A versatile Mössbauer analysis program. Uppsala University, Institute of Physics, Sweden (UIIP-1090).

MacDonald, D.J. and Hawthorne, F.C. (1995) Cu-bearing tourmaline from Paraíba, Brazil. *Acta Crystallographica*, C51, 555–557.

Mattson, S.M. and Rossman, G.R. (1984) Ferric iron in tourmaline. *Physics and Chemistry of Minerals*, 11, 225–234.

North, A.C.T., Phillips, D.C., and Mathews, F.S. (1968) A semi-empirical method of absorption correction. *Acta Crystallographica*, A24, 351–359.

Oliveira, E.O., Castañeda, C., Eeckhout, S.G., Gilmar, M.M., Kwitko, R.R., De Grave, E., and Botelho, N.F. (2002) Infrared and Mössbauer study of Brazilian tourmalines from different geological environments. *American Mineralogist*, 87, 1154–1163.

Pieczka, A. (2000) Modeling of some structural parameters of tourmalines on the basis of their chemical composition. I. Ordered structure model. *European Journal of Mineralogy*, 12, 589–596.

Pieczka, A. and Krazcka, J. (2004) Oxidized tourmalines—a combined chemical, XRD and Mössbauer study. *European Journal of Mineralogy*, 16, 309–321.

Pouchou, J.L. and Pichoir, F. (1984) A new model for quantitative X-ray microanalysis. I. Application to the analysis of homogeneous samples. *La Recherche Aérospatiale*, 3, 13–36.

Robinson, K., Gibbs, G.V., and Ribbe, P.H. (1971) Quadratic elongation: A quantitative measure of distortion in coordination polyhedra. *Science*, 172, 567–570.

Selway, J.B., Smeds, S.A., Černý, P., and Hawthorne, F.C. (2002) Compositional evolution of tourmaline in the petalite-subtype Nyköpinggruvan pegmatites, Utö, Stockholm Archipelago, Sweden. *GFF*, 124, 93–102.

Sheldrick, G.M. (1997) SHELXL-97-1. Program for crystal structure determination. University of Göttingen, Germany.

Stålhös, G. (1982) Beskrivning till berggrundskartan Nynäshamn NO/SO. Utö med omgivande skärgård. Sveriges Geologiska Undersökning, Af 138, 1–124.

Zhe, L. and De Grave, E. (1998) The Fe²⁺ quadrupole splitting at octahedral sites in chain silicates: Correlations with the site-distortion parameters. *Hyperfine Interactions*, 116, 173–178.

MANUSCRIPT RECEIVED JUNE 19, 2007

MANUSCRIPT ACCEPTED APRIL 25, 2008

MANUSCRIPT HANDLED BY DARRELL HENRY